

Design of error-compensating algorithms for sinusoidal phase shifting interferometry

Peter de Groot

Zygo Corporation, Laurel Brook Road, Middlefield, Connecticut 06457, USA
(peterd@zygo.com)

Received 12 August 2009; revised 3 November 2009; accepted 5 November 2009;
posted 10 November 2009 (Doc. ID 115548); published 3 December 2009

An improved approach to interferometry using sinusoidal phase shifting balances several harmonic components in the interference signal against each other. The resulting computationally efficient phase-estimation algorithms have low sensitivity to errors such as spurious intensity noise, vibration, and errors in the phase shift pattern. Specific example algorithms employing 8 and 12 camera frames illustrate design principles that are extendable to algorithms of any length for applications that would benefit from a simplified, sinusoidal phase shift. © 2009 Optical Society of America

OCIS codes: 120.3180, 120.3930, 120.4640, 120.5050, 120.5060, 180.3170.

1. Introduction

Interferometers for distance measurement and surface profiling often employ a phase shifting technique to determine interference phase [1]. An alternative to the conventional linear phase shift is a sinusoidal phase shift, which has the benefit of relaxing requirements on the phase shifting device. A sinusoidal phase shift is easier to implement in many practical systems, and facilitates high-speed, continuous data averaging, which increases performance in the presence of electronic, optical, and environmental noise.

Algorithms for sinusoidal phase shifting interferometry (sinusoidal PSI) have a form similar to the more familiar linear phase shifting interferometry (linear PSI) algorithms. A pioneering example is the Sasaki four-frame sinusoidal PSI algorithm published in 1987, which reads

$$\tan(\theta) = \frac{I_0 + I_1 - I_2 - I_3}{I_0 - I_1 + I_2 - I_3}, \quad (1)$$

where the $I_{0,1,2,3}$ are interference intensity samples acquired sequentially during a complete sinusoidal

phase shift cycle [2,3]. From the appearance of this algorithm, it is clear that sinusoidal PSI does not present any special computation problems when compared to linear PSI, which employs algorithms of the same basic form. Indeed, sinusoidal PSI has been shown to be effective for various instruments from Fizeau interferometers [4] to interference microscopes [5,6]. Nonetheless, sinusoidal PSI has not enjoyed nearly the same popularity as linear PSI. Part of the reason for this is the vast literature on linear PSI and the extensive catalog of error-compensating algorithms that have grown out of this analysis.

The present work takes a second look at sinusoidal PSI, with the goal of developing a class of error-compensating algorithms to enhance its range of application [7,8]. Error compensation is achieved by summing the contributions of several of the harmonic components of the interference signal in a way that automatically balances error contributions. The conclusion is that sinusoidal PSI can be significantly improved in robustness while retaining the benefits of simplified phase shifting.

2. Sinusoidal Phase Shifting

The laser Fizeau interferometer of Fig. 1 serves as an example instrument for developing the concepts for sinusoidal phase shifting. The instrument determines a

0003-6935/09/356788-09\$15.00/0
© 2009 Optical Society of America

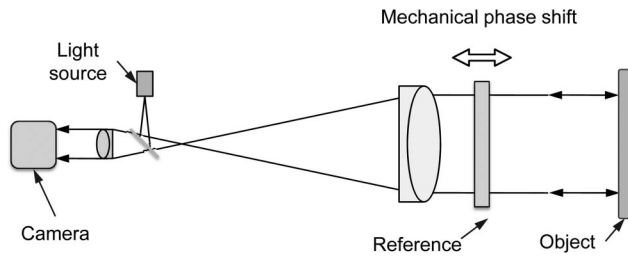


Fig. 1. Laser Fizeau interferometer for optical testing. Mechanical motion of approximately 1 micron excursion introduces controlled phase shifts while the camera captures a sequence of interference patterns.

height h at multiple positions in the field of view from the interference phase θ at a wavelength λ :

$$\theta = 4\pi h/\lambda. \quad (2)$$

The phase is detected from the detected interference intensity

$$I(\theta, t) = q\{1 + V \cos[\theta + \phi(t)]\}, \quad (3)$$

where V is the fringe visibility, q is the average intensity, and $\phi(t)$ is a controlled phase shift. In sinusoidal PSI, the phase shift can be expressed as a cosine of amplitude u :

$$\phi(t) = u \cos[\alpha(t) + \varphi], \quad (4)$$

where

$$\alpha(t) = 2\pi f t. \quad (5)$$

Here f is a frequency and φ is a timing offset related to the triggering of the phase shift with respect to the camera. I have chosen a cosine instead of a sine in Eq. (4) so that the phase shift is symmetric about zero when the timing offset φ is zero, as shown in Figs. 2 and 3.

Using the phase α in place of the time variable, the intensity in Eq. (3) expands to

$$I(\theta, \alpha) = q + qV \cos(\theta) \cos[\phi(\alpha)] - qV \sin(\theta) \sin[\phi(\alpha)]. \quad (6)$$

From the real and imaginary parts of the Jacobi-Anger expansion [9],

$$\exp[iu \cos(\alpha)] = J_0(u) + 2 \sum_{\nu=1}^{\infty} i^\nu J_\nu(u) \cos(\nu\alpha), \quad (7)$$

the intensity (6) is rewritten as

$$I(\theta, \alpha) = qD(\theta) + qV \cos(\theta)C(\alpha) + qV \sin(\theta)S(\alpha), \quad (8)$$

where

$$D(\theta) = 1 + VJ_0(u) \cos(\theta), \quad (9)$$

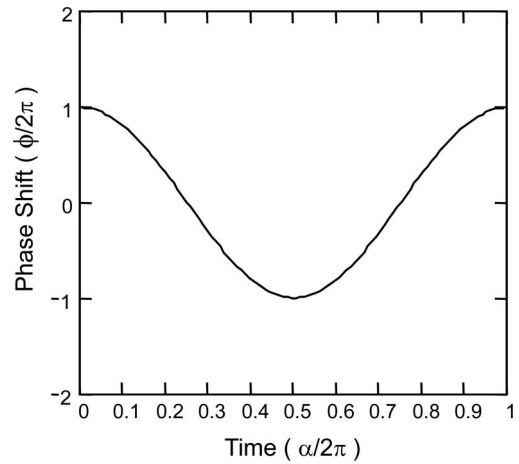


Fig. 2. Sinusoidal phase shift $\phi(\alpha)$ for a phase shift amplitude $u = \pi$ and $\varphi = 0$.

$$S(\alpha) = 2 \sum_{\nu=1,3,5,\dots}^{\infty} (-1)^{(\nu+1)/2} J_\nu(u) \cos[\nu(\alpha + \varphi)], \quad (10)$$

$$C(\alpha) = 2 \sum_{\nu=2,4,6,\dots}^{\infty} (-1)^{\nu/2} J_\nu(u) \cos[\nu(\alpha + \varphi)], \quad (11)$$

and the J_ν are Bessel functions, as shown in Fig. 4. The time-dependent portion of the intensity signal is therefore a sum of harmonics ν of the fundamental phase shift frequency.

Detection of the intensity signal requires collecting photons over a dwell time or integrating bucket, effectively averaging the signal over a portion of the phase shift. The mean value of the intensity at the phase shift phase α averaged over the interval β is

$$\bar{I}(\theta, \alpha) = \int_{\alpha-\beta/2}^{\alpha+\beta/2} I(\theta, \alpha') d\alpha', \quad (12)$$

where $I(\theta, \alpha')$ is the instantaneous intensity as given by Eq. (8), and α' is the variable of integration over

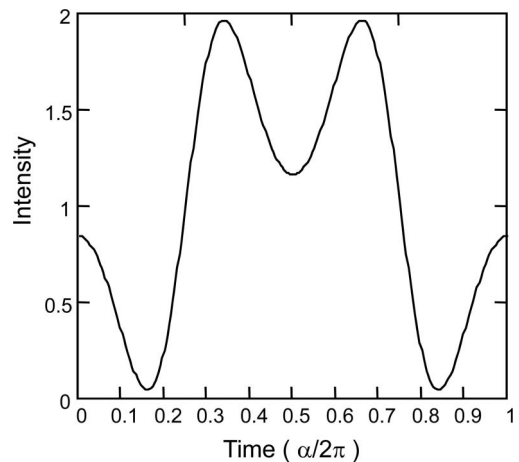


Fig. 3. Interference signal $I(\alpha)$ resulting from the sinusoidal phase shift $\phi(\alpha)$ shown in Fig. 2 for an interference phase $\theta = \pi/2$.

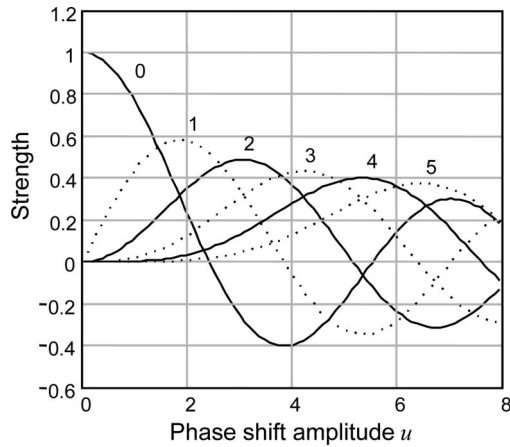


Fig. 4. Strength of even (solid lines) and odd (dashed lines) harmonics in the SinPSI signal as a function of the sinusoidal phase shift amplitude u .

the dwell time expressed as the phase interval β . The effect of the frame integration is to attenuate the higher frequency harmonics by a factor

$$B(\nu) = \frac{\sin(\nu\beta/2)}{\nu\beta/2}. \quad (13)$$

The intensity signal is now

$$\bar{I}(\theta, \alpha) = qD(\theta) + qV \cos(\theta)\bar{C}(\alpha) + qV \sin(\theta)\bar{S}(\alpha), \quad (14)$$

where $D(\theta)$ is as in Eq. (9), and

$$\bar{S}(\alpha) = 2 \sum_{\nu=1,3,5,\dots}^{\infty} (-1)^{(\nu+1)/2} B(\nu) J_{\nu}(u) \cos[\nu(\alpha + \varphi)], \quad (15)$$

$$\bar{C}(\alpha) = 2 \sum_{\nu=2,4,6,\dots}^{\infty} (-1)^{\nu/2} B(\nu) J_{\nu}(u) \cos[\nu(\alpha + \varphi)]. \quad (16)$$

3. Phase Detection

The phases of the harmonics $\cos[\nu(\alpha + \varphi)]$ in Eqs. (15) and (16) are independent of the interference phase θ . Thus, unlike linear phase shifting, we do not determine θ from the analysis of the phases of periodic components of the signal $\bar{I}(\theta, \alpha)$. Rather, in sinusoidal PSI, the strategy is to evaluate the strengths of the odd and even harmonics.

A frequency analysis of the signal $\bar{I}(\theta, \alpha)$ acquired over a range of phase shifts would allow us to calculate the strengths of the odd and of the even harmonics. Inspection of Eq. (14) shows that the odd harmonics vary as $\sin(\theta)$ and the even harmonics vary as $\cos(\theta)$. The phase θ follows therefore from the ratio of the strengths of the odd and even harmonics, after properly normalizing for $\bar{S}(\alpha)$ and $\bar{C}(\alpha)$. A straightforward way to perform the required fre-

quency analysis would be a complete complex Fourier transform to directly view the frequency content. However, a full Fourier analysis requires dense sampling to avoid aliasing and a software procedure that is unnecessarily intensive.

Some *a priori* information leads to a calculation that is as computationally efficient as comparable algorithms for linear phase shifting.

First, the frequencies of all of the harmonics appearing in the intensity data are well known because they are tied to the fundamental sinusoidal phase shift frequency f provided by the phase shifting electronics. These frequencies have nothing to do with the measuring geometry, the wavelength, or any other attribute of the interference measurement, and can be established with almost arbitrary precision. Therefore it is not necessary to search through a continuum of frequencies to locate the harmonics—it is only required to measure the strengths of specific frequencies that are integer multiples of the fundamental.

Second, for phase shift amplitudes of 2π or less, only the first few harmonics are of significant strength. Thus we need only identify and Fourier analyze a handful of fixed, low-frequency harmonics that we wish to use.

Third, because the timing offset φ is a fixed value characteristic of the electronic timing of the sinusoidal phase shifting drive signal, it is not necessary to solve simultaneously for the magnitude and phase of the harmonic components in the interference signal. It follows that we are free to set the timing offset φ to any convenient fixed value. In this paper, I set $\varphi = 0$ so that the signal $\bar{I}(\theta, \alpha)$ includes only cosine functions that are symmetric about $\alpha = 0$. The coefficients of a complex Fourier analysis are then purely real, and we need only perform the cosine portion of the Fourier analysis.

Using these simplifications, define a sequence of P phases α_j of the sinusoidal phase shift spaced by $\Delta\alpha = 2\pi/P$ and starting at a sampling offset $\alpha_0 = \pi/P$:

$$\phi_j = u \cos(\alpha_j), \quad (17)$$

$$\alpha_j = j\Delta\alpha + \alpha_0, \quad (18)$$

$$j = 0, 1, 2, \dots, P-1. \quad (19)$$

Most often, the phase interval β is also equal to the phase increment $\Delta\alpha$. The frequency analysis follows from the normalized, real-valued Fourier-cosine transform

$$H(\theta, \nu) = \frac{\sum_j \cos(\nu\alpha_j) \bar{I}_j(\theta)}{\sum_j \cos(\nu\alpha_j)^2} \quad (20)$$

for a given frequency ν . We expect from Eqs. (15) and (16) that the relevant frequencies are at specific

integer harmonics indexed by ν . Let us define therefore a normalized sampling vector

$$h_{\nu,j} = \frac{\cos(\nu\alpha_j)}{\sum_j \cos(\nu\alpha_j)^2} \quad (21)$$

to detect the θ -dependent amplitude of the cosine at the discrete harmonic ν , which is now an integer index for the harmonic $H_\nu(\theta)$:

$$H_\nu(\theta) = \sum_j h_{\nu,j} \bar{I}_j(\theta). \quad (22)$$

Sparse sampling means that the single-frequency transform $H_\nu(\theta)$ will be sensitive to higher integer frequencies than just the selected value ν because of aliasing. We require therefore that the sampling vectors h be sensitive only to even or odd harmonics, as the case may be. We further require that

$$\sum_j h_{\nu,j} = 0, \quad (23)$$

which is equivalent to the requirement that the DC portion of the signal have no influence on the result. Note that the sampling vector definition Eq. (21) and the choice of α in Eq. (18) ensure that Eq. (23) is satisfied.

As an example, one approach would be to compare the first harmonic $H_1(\theta)$ to the second harmonic $H_2(\theta)$ to determine θ . With some differences in assumptions and notation, this is essentially the foundation of the 1987 Sasaki method. Unfortunately, using only these two harmonics leads to a high sensitivity to error when compared to modern error-compensating linear phase shift algorithms. As a specific example, the Sasaki algorithm is 20× more sensitive to a 10% error in phase shifter calibration than the well known Schwider–Hariharan linear PSI algorithm [10].

4. Balancing Multiple Harmonics to Improve Performance

There are many known techniques for improving performance in conventional linear PSI through the development of error-compensating algorithms. These include Fourier transform windows, characteristic polynomials, extended averaging, self-calibration, and so on, as summarized in Ref. [1]. Unfortunately, none of these methods are of any relevance for improving sinusoidal PSI algorithms.

I propose here to improve the robustness of phase detection in sinusoidal phase shifting by taking advantage of the many harmonics present in the interference signal of Eq. (14) to balance the results in the presence of errors. To this end, we sum a series of coefficient vectors h_ν for two or more harmonic frequencies ν using weights γ_ν to obtain vectors h_{odd} , h_{even} :

$$h_{\text{odd},j} = \sum_{\nu=\text{odd}} \gamma_\nu h_{\nu,j}, \quad (24)$$

$$h_{\text{even},j} = \sum_{\nu=\text{even}} \gamma_\nu h_{\nu,j}. \quad (25)$$

These summed harmonics lead to values that are representative of the relative strengths of the odd and even harmonics, respectively:

$$H_{\text{odd}}(\theta) = \sum_j h_{\text{odd},j} \bar{I}_j(\theta), \quad (26)$$

$$H_{\text{even}}(\theta) = \sum_j h_{\text{even},j} \bar{I}_j(\theta). \quad (27)$$

Note that properly designed coefficient vectors h_{odd} , h_{even} are orthogonal,

$$\sum_j h_{\text{odd},j} h_{\text{even},j} = 0, \quad (28)$$

and are sensitive only to the appropriate harmonics:

$$\sum_j h_{\text{odd},j} \cos(\nu\alpha_j) = 0 \quad \text{for } \nu = 2, 4, 6, \dots, \quad (29)$$

$$\sum_j h_{\text{even},j} \cos(\nu\alpha_j) = 0 \quad \text{for } \nu = 1, 3, 5, \dots \quad (30)$$

Assuming that these conditions are met, the phase θ follows from the quadrature formula

$$\tan(\theta) = \frac{\Gamma_{\text{even}} H_{\text{odd}}(\theta)}{\Gamma_{\text{odd}} H_{\text{even}}(\theta)} \quad (31)$$

that includes normalization constants Γ_{odd} , Γ_{even} calculated from the ideal signal Eqs. (15) and (16) for a specific phase shift amplitude $u = u_0$ and offset $\varphi = 0$:

$$\Gamma_{\text{odd}} = 2 \sum_{\nu=1,3,5,\dots}^{\infty} (-1)^{(\nu+1)/2} J_\nu(u_0) B(\nu) \sum_j h_{\text{odd},j} \cos(\nu\alpha_j), \quad (32)$$

$$\Gamma_{\text{even}} = 2 \sum_{\nu=2,4,6,\dots}^{\infty} (-1)^{\nu/2} J_\nu(u_0) B(\nu) \sum_j h_{\text{even},j} \cos(\nu\alpha_j). \quad (33)$$

The design flow is as follows:

1. Select a series of harmonics indexed by ν to be included in the algorithm.
2. Calculate the corresponding vectors $h_{\nu,j}$ using Eq. (21) for a sequence of P phases α_j , as in Eq. (18).

3. Sum the vectors $h_{\nu,j}$ using weights γ_ν to construct final coefficients h_{odd} , h_{even} according to Eqs. (24) and (25). The algorithm design centers on the choice of these weights γ_ν and of the phase-shift amplitude u_0 .

4. Calculate the normalization constants Γ_{odd} , Γ_{even} using Eqs. (32) and (33).

5. Use Eq. (31) to calculate the phase θ .

5. Evaluation Functions to Guide Algorithm Design

The previous section provides the essential toolbox for generating new algorithms, apart for one missing tool: a means to provide feedback and direction in the design process so as to arrive at the optimum set of algorithm coefficients.

Although there are many different error sources in interferometers, the error propagation for sinusoidal phase shifting can in most cases be analyzed by evaluation of the sensitivity of the algorithm to the phase shift amplitude u defined in Eq. (4). The sensitivity of the sine (odd-harmonic) and cosine (even-harmonic) portions of the quadrature function in Eq. (31) map through the normalization constants Γ_{odd} , Γ_{even} , and will be incorrect if the amplitude u differs from the design value u_0 .

Let us define therefore the following *filter functions*:

$$F_{\text{odd}}(u) = 2 \sum_{\nu=1,3,5,\dots}^{\infty} (-1)^{(\nu+1)/2} J_\nu(u) B(\nu) \sum_j h_{\text{odd},j} \cos(\nu\alpha_j), \quad (34)$$

$$F_{\text{even}}(u) = 2 \sum_{\nu=2,4,6,\dots}^{\infty} (-1)^{\nu/2} J_\nu(u) B(\nu) \sum_j h_{\text{even},j} \cos(\nu\alpha_j), \quad (35)$$

which show the sensitivity to phase shift amplitude u of the numerator and denominator, respectively, in the quadrature formula Eq. (31) for θ . The functions F_{odd} , F_{even} are the same as the constants Γ_{odd} , Γ_{even} given in Eqs. (32) and (33) apart from the replacement of the fixed value u_0 with the variable value u . Thus when $u = u_0$,

$$\Gamma_{\text{odd}} = F_{\text{odd}}(u_0), \quad (36)$$

$$\Gamma_{\text{even}} = F_{\text{even}}(u_0). \quad (37)$$

The term *filter function* is intentionally analogous to functions of the same name but of an entirely different form often used to guide algorithm design for linear phase shifts [11].

As an illustration of how these functions work, consider a simple, non error compensating algorithm based only on the first two harmonics $\nu = 1$ and $\nu = 2$ and just 4 sample shifts

$$\alpha_j = j\pi/2 \quad (38)$$

for $j = 0, 1, 2, 3$. Using Eq. (21) and setting $\gamma_1 = -2$, $\gamma_2 = -4$, the algorithm coefficients are

$$h_{\text{odd}} = (-1 \ 0 \ 1 \ 0), \quad (39)$$

$$h_{\text{even}} = (-1 \ 1 \ -1 \ 1). \quad (40)$$

The normalization constants from Eqs. (32) and (33) for a phase shift excursion $u_0 = 2.45$ are

$$\Gamma_{\text{odd}} = 1.5718, \quad (41)$$

$$\Gamma_{\text{even}} = 2.2283, \quad (42)$$

and the phase calculation of Eq. (31) simplifies to

$$\tan(\theta) = 1.4176 \frac{\bar{I}_0 - \bar{I}_2}{\bar{I}_0 - \bar{I}_1 + \bar{I}_2 - \bar{I}_3}. \quad (43)$$

This algorithm has similar characteristics as the Sasaki 1987 algorithm [2], but with a zero phase offset φ .

Figure 5 shows the behavior of the two filter functions $F_{\text{odd}}(u)$ and $F_{\text{even}}(u)$ plotted as a function of the sinusoidal phase shift amplitude u for the 4-frame algorithm of Eq. (43). The two curves are normalized to the constants Γ_{odd} and Γ_{even} , respectively, so that the curves are equal to one at the design amplitude $u_0 = 2.45$. What is most evident is that the curves diverge rapidly when the amplitude u moves away from the design amplitude u_0 . This shows that the ratio of the numerator to the denominator in Eq. (43) is an unstable function of u . Among other things, this explains why an algorithm based only on the first two harmonics $\nu = 1 \ \nu = 2$ requires a precise calibration of the phase shift amplitude. A further observation is that the filter functions show high sensitivity to sinusoidal modulation amplitudes far from the design amplitude $u_0 = 2.45$, which makes the algorithm sensitive to spurious phase modulations and noise.

From these observations, we can infer the following design rules: First, the normalized filter functions $F_{\text{odd}}/\Gamma_{\text{odd}}$ and $F_{\text{even}}/\Gamma_{\text{even}}$ should be near maximum, matched in value, and matched in derivative at the design amplitude u_0 . Second, the filter functions should have low values far from the design amplitude u_0 , particularly at integer multiples of u_0 , so as to reduce sensitivity to nonlinearities in the phase shift and in the detector. Following these two basic design rules leads to robustness and error resistance.

6. Error-Compensating Algorithms

As one would expect, the ability to shape the filter functions $F_{\text{odd}}(u)$ and $F_{\text{even}}(u)$ depends on how many harmonics are available, a number that increases with increased sample number P . Higher numbers of harmonics also allows for additional constraints and higher performance.

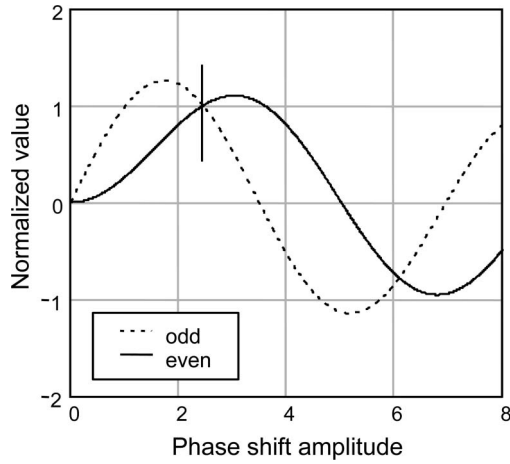


Fig. 5. Variation in the normalized filter functions $F_{\text{odd}}/\Gamma_{\text{odd}}$ and $F_{\text{even}}/\Gamma_{\text{even}}$ as a function of the sinusoidal phase shift amplitude u for the 4-frame sinusoidal PSI algorithm in Eq. (43). The design amplitude u_0 is shown by the vertical line at 2.35 rad.

As a first example, an 8-frame algorithm shows how to include just one additional harmonic to achieve a significant improvement. To detect and balance harmonics $\nu > 2$, a $\Delta\alpha = \pi/4$ step moves the Nyquist frequency from 2 to 4, giving us greater control over the relative weighting of the first and third harmonics. The data acquisition pattern as illustrated in Fig. (6) is now

$$\alpha_j = j\pi/4 + \pi/8 \quad (44)$$

for $j = 0, 1, \dots, 7$. Using Eq. (21) for the first, second, and third harmonics,

$$h_1 = \frac{1}{4}[\varsigma_1 \quad \varsigma_3 \quad -\varsigma_3 \quad -\varsigma_1 \quad -\varsigma_1 \quad -\varsigma_3 \quad \varsigma_3 \quad \varsigma_1], \quad (45)$$

$$h_2 = \frac{1}{4\sqrt{2}}(1 \quad -1 \quad -1 \quad 1 \quad 1 \quad -1 \quad -1 \quad 1), \quad (46)$$

$$h_3 = \frac{1}{4}[\varsigma_3 \quad -\varsigma_1 \quad \varsigma_1 \quad -\varsigma_3 \quad -\varsigma_3 \quad \varsigma_1 \quad -\varsigma_1 \quad \varsigma_3], \quad (47)$$

where

$$\varsigma_1 = \cos(\pi/8), \quad (48)$$

$$\varsigma_3 = \cos(3\pi/8). \quad (49)$$

We choose the weights γ_ν and the design amplitude u_0 either by mathematical optimization or interactivity, using a real-time visual display of $F_{\text{odd}}(u)$ and $F_{\text{even}}(u)$. A convenient starting point for the 8-frame algorithm is to set

$$\gamma_1 = -4\varsigma_3/(\varsigma_1^2 + \varsigma_3^2), \quad (50)$$

$$\gamma_2 = -4\sqrt{2}, \quad (51)$$

$$\gamma_3 = 4\varsigma_1/(\varsigma_1^2 + \varsigma_3^2), \quad (52)$$

so that we have simple, integer-coefficient vectors

$$h_{\text{odd}} = (0 \quad -1 \quad 1 \quad 0 \quad 0 \quad 1 \quad -1 \quad 0), \quad (53)$$

$$h_{\text{even}} = (-1 \quad 1 \quad 1 \quad -1 \quad -1 \quad 1 \quad 1 \quad -1). \quad (54)$$

The next step is to choose a phase shift excursion u_0 that at the same time provides high signal strength and stable agreement between the normalized functions $F_{\text{odd}}/\Gamma_{\text{odd}}$ and $F_{\text{even}}/\Gamma_{\text{even}}$ near the design amplitude u_0 . A value near $u_0 = 2.93$ is close to the maximum values of $F_{\text{odd}}/\Gamma_{\text{odd}}$ and $F_{\text{even}}/\Gamma_{\text{even}}$ and at the same time provides a match for the derivatives of these two functions. The normalizations from Eqs. (32) and (33) are

$$\Gamma_{\text{odd}} = 2.9432, \quad (55)$$

$$\Gamma_{\text{even}} = 4.8996, \quad (56)$$

$$\Gamma_{\text{even}}/\Gamma_{\text{odd}} = 1.6647. \quad (57)$$

Using the inherent symmetry of the data acquisition (see Fig. 6), the phase estimation in Eq. (31) simplifies to

$$\tan(\theta) = \frac{1.6647(g_1 - g_2)}{-g_0 + g_1 + g_2 - g_3}, \quad (58)$$

where we average symmetric camera frames according to

$$g_j = \bar{I}_j + \bar{I}_{7-j}; \quad j = 0, 1, 2, 3. \quad (59)$$

The behavior of $F_{\text{odd}}(u)$ and $F_{\text{even}}(u)$ shown in Fig. 7 confirms that the 8-frame sinusoidal PSI algorithm using three harmonics $\nu = 1, 2, 3$ is much more stable with phase shift amplitude u than an algorithm based on only the two harmonics $\nu = 1, 2$. Specifically, the first derivatives of $F_{\text{odd}}/\Gamma_{\text{odd}}$ and $F_{\text{even}}/\Gamma_{\text{even}}$ are identical at u_0 for Fig. 7, whereas they are opposite for Fig. 5. One consequence is that the phase error for the 8-frame sinusoidal PSI algorithm with a phase shifter calibration error of 10% is only 0.34° rms compared to 5° rms for the 4-frame algorithm, an improvement of more than an order of magnitude.

Following a similar interactive optimization, the following 12-frame algorithm based on the first five harmonics, $\nu = 1, 2, \dots, 5$, has a phase increment $\Delta\alpha = \pi/6$ and a sampling offset $\alpha_0 = \pi/12$:

$$\tan(\theta) = \frac{1.2461(g_0 - g_5) - 1.5525(g_1 - g_4) - 2.5746(g_2 - g_3)}{0.2707(g_0 + g_5) - 2.6459(g_1 + g_4) + 2.3753(g_2 + g_3)}, \quad (60)$$

where now we average symmetric camera frames according to

$$g_j = \bar{I}_j + \bar{I}_{11-j}; \quad j = 0, 1, 2, 3. \quad (61)$$

As shown in Fig. 8, the normalized filter functions $F_{\text{odd}}/\Gamma_{\text{odd}}$ and $F_{\text{even}}/\Gamma_{\text{even}}$ follow each other very closely over a broad range about the design amplitude $u_0 = 3.384$. For this algorithm, u_0 is intentionally not quite at the peak sensitivity of the curves $F_{\text{odd}}/\Gamma_{\text{odd}}$ and $F_{\text{even}}/\Gamma_{\text{even}}$ so that $F_{\text{odd}} = 0$ and $F_{\text{even}} = 0$ at $u = 2u_0$, thereby reducing sensitivity to several error sources that generate false phase modulations, including, in particular, quadratic nonlinearity in the detector and multiple reflections within Fizeau cavities.

Assuming that we allow that the algorithm coefficients do not need to be integers, there is an infinite variety of solutions based on how much emphasis is placed on certain algorithm features. Sinusoidal PSI algorithms for 8, 10, 12, 14, 16, and 20 camera frames have been derived in this way using the harmonic balance method, generally with increasingly good performance as the number of camera frames increases.

7. Error Sensitivity

References [7,8] provide analytical formulas for a wide range of error sources for sinusoidal phase shifting interferometry. Here I present a few key results using the 4-, 8-, and 12-frame algorithms as examples.

A. Phase Shift Calibration

A classic performance criterion for PSI is sensitivity to deviations in the phase shift excursion from the expected or optimal value. Some of these variations

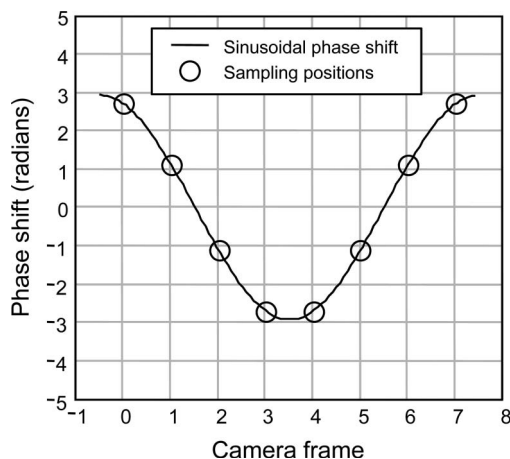


Fig. 6. Data acquisition pattern for the 8-frame algorithm.

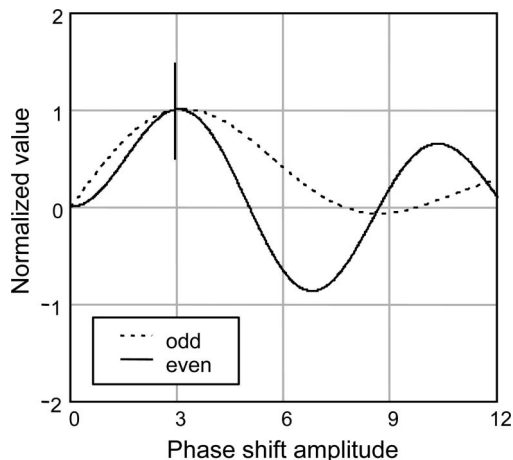


Fig. 7. Variation in the normalized filter functions $F_{\text{odd}}/\Gamma_{\text{odd}}$ and $F_{\text{even}}/\Gamma_{\text{even}}$ as a function of the sinusoidal phase shift amplitude u for the 8-frame sinusoidal PSI algorithm in Eq. (43). The design amplitude u_0 is shown by the vertical line at 2.95 rad.

are inevitable—in a high-NA spherical Fizeau cavity with a mechanical phase shifting mechanism, the phase shift excursion varies as a function of angle.

The standard deviation of the phase error ε from phase shift calibration error δu is

$$\varepsilon_{\text{stdv}}(\delta u) = \frac{1}{2\sqrt{2}} |\rho(\delta u) - 1|, \quad (62)$$

where

$$\rho(\delta u) = \frac{F_{\text{even}}(u_0 + \delta u) \Gamma_{\text{odd}}}{F_{\text{odd}}(u_0 + \delta u) \Gamma_{\text{even}}}. \quad (63)$$

The error is cyclic at twice the rate of θ , just as in linear phase shifting. Figure 9 summarizes the magnitude of the error for the 4-, 8-, and 12-frame algorithms.

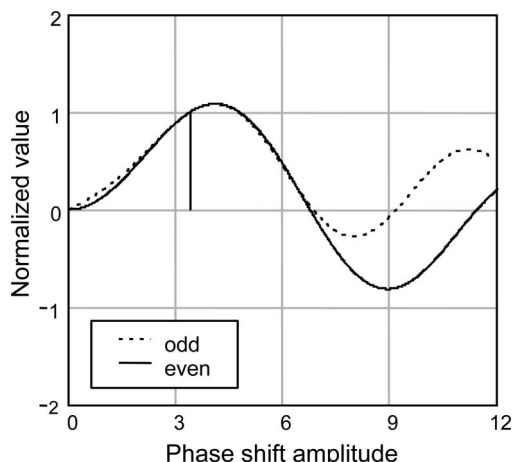


Fig. 8. Variation in the normalized filter functions $F_{\text{odd}}/\Gamma_{\text{odd}}$ and $F_{\text{even}}/\Gamma_{\text{even}}$ as a function of the sinusoidal phase shift amplitude u for the 12-frame sinusoidal PSI algorithm in Eq. (60). The design amplitude u_0 shown by the vertical line at 3.384 rad is positioned so that the algorithm sensitivity is zero at $u = 2u_0 = 6.768$.

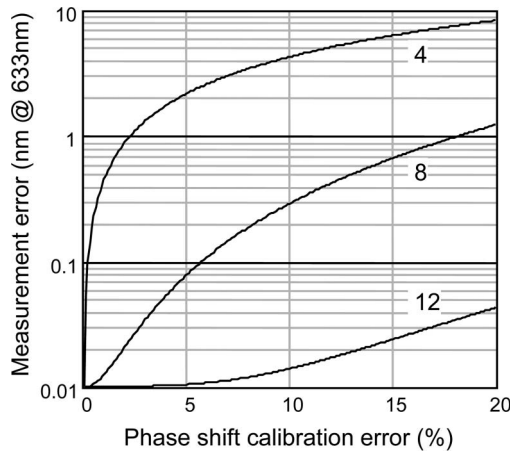


Fig. 9. Measurement error in nm rms over a full cycle of phase at 633 nm wavelength as a function of calibration error, for algorithms based on 4, 8, and 12 camera frames per sinusoidal phase shift cycle.

B. Additive Random Noise

Random noise changes the interference intensity signal from Eq. (3) to

$$I(\theta, t) = q\{1 + V \cos[\theta + \phi(t)]\} + n(\sigma, t), \quad (64)$$

where σ is the rms of the random noise $n(\sigma, t)$. A mathematical analysis of additive random noise for SinPSI leads to the following formula for the rms phase error:

$$\varepsilon_{\text{rms}} = \left(\frac{\sigma}{qV}\right) \frac{1}{\sqrt{2}} \sqrt{\left(\frac{p_{\text{even}}}{\Gamma_{\text{even}}}\right)^2 + \left(\frac{p_{\text{odd}}}{\Gamma_{\text{odd}}}\right)^2}, \quad (65)$$

where

$$p_{\text{odd}} = \sqrt{\sum_j (h_{\text{odd}})_j^2}, \quad (66)$$

$$p_{\text{even}} = \sqrt{\sum_j (h_{\text{even}})_j^2}. \quad (67)$$

The summary results of Table 1 tell us the expected rms phase error ε_{rms} for an rms noise level σ/qV . The tabulated results are scaled by $633 \text{ nm}/4\pi$. As expected, the sensitivity to noise declines with the number of camera frames, approximately at the rate of the square root of the number of frames. This is a similar result to conventional linear phase shifting.

Table 1. Error in nm rms Over a Full Phase Cycle at 633 nm for 1% Random Noise

Frames	Error (nm)
4	0.45
8	0.32
12	0.29

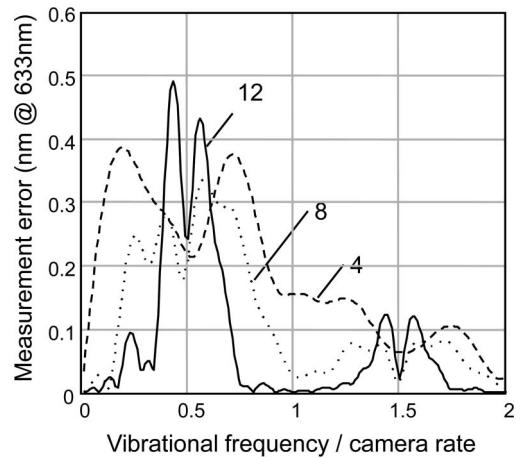


Fig. 10. Sensitivity of the 4-, 8-, and 12-frame sinusoidal PSI algorithms to a 1 nm vibrational amplitude. The measurement error in nm rms over a full cycle of phase at 633 nm wavelength is plotted as a function of vibrational frequency normalized to the camera frame rate.

C. Vibration

Because the data acquisition takes place over time, sensitivity to vibration can be an issue for PSI. Given a pure, single-frequency vibration, the intensity modifies to

$$I(\theta, \alpha, \nu') = q\{1 + V \cos[\theta + \phi(\alpha) + n(\alpha, \nu')]\}, \quad (68)$$

where for a vibrational frequency ν' , rms σ , and phase ξ , the vibration is

$$n(\alpha, \nu') = \sqrt{2}\sigma \times \cos[\nu'\alpha + \xi]. \quad (69)$$

The error propagation for vibration can be calculated analytically for small vibrational amplitudes, as reported in Refs. [7,8]. Figure 10 shows that the simple 4-frame SinPSI algorithm has a high sensitivity to vibration over a broad frequency range; however, the error-compensating 8- and 12-frame algorithms are much improved. The 12-frame algorithm has similar behavior to linear PSI, both in the frequency bandwidth and the peak sensitivity near one-half the camera rate [12].

D. Detector Nonlinearity

A nonlinearity of order $n \geq 2$ of a detector or camera may be defined by

$$\Delta I = q\zeta \left[\left(\frac{I-q}{q}\right)^2 - \frac{1}{2} \right] \left(\frac{I-q}{q}\right)^{(n-2)}, \quad (70)$$

Table 2. Error in nm rms Over a Full Phase Cycle at 633 nm for a 1% Detector Nonlinearity of Order n

Frames	$n = 2$	$n = 3$	$n = 4$
4	0.22	0.13	0.17
8	0.17	0.11	0.12
12	0.03	0.15	0.13

Table 3. Error in nm rms Over a Full Phase Cycle at 633 nm for a 1% Phase Shift Nonlinearity of Order n

Frames	$n = 2$	$n = 3$	$n = 4$
4	0.14	0.22	0.04
8	0.19	0.12	0.13
12	0.01	0.04	0.02

where ΔI refers to the deviation with respect to a linear fit to the detected signal I , and q is the mean intensity. Note that ζ is the peak–valley (P–V) departure from linear over the full dynamic range of the detector.

Detector nonlinearity is a particularly complex error source in sinusoidal PSI, generating a large spectrum of harmonics. Table 2 shows a significant improvement in resistance to quadratic nonlinearity when using the 12-frame sinusoidal PSI algorithm compared to the 4-frame algorithm. The improvement relates to constructing the algorithm so that the filter functions F_{odd} , F_{even} are both zero at twice the design phase shift amplitude $u = 2u_0$ (see Fig. 8). Suppression of the cubic nonlinearity sensitivity is also possible by suppressing F_{odd} , F_{even} at $u = 3u_0$, using an algorithm with >12 camera frames per sinusoidal phase shift cycle to bring more harmonics into the algorithm design.

E. Phase Shift Nonlinearity

A heavily loaded mechanical phase shifter or low-voltage piezoactuator can have a nonlinear response, leading to a distorted phase shift. Similarly to Eq. (70), a nonlinear phase shift may be written as a polynomial of order $n \geq 2$ using

$$\Delta\phi = u\zeta \left[\left(\frac{\phi - \langle\phi\rangle}{u} \right)^2 - \frac{1}{2} \right] \left(\frac{\phi - \langle\phi\rangle}{u} \right)^{(n-2)}, \quad (71)$$

where $\Delta\phi$ refers to the deviation with respect to a linear fit to the desired phase shift ϕ , $\langle\phi\rangle$ is the mean phase, u is the phase shift amplitude, and ζ is the P–V departure from linear. The results of numerical calculations for phase shift nonlinearity in Table 3 once again show significantly improved performance with error-compensating sinusoidal PSI.

8. Discussion and Conclusion

Sinusoidal PSI is of greatest interest when the limiting hardware is the phase shift mechanism. A relevant application is high-speed, continuous data averaging with a mechanical phase shifter or any other device with limited frequency response. The sinusoidal shift pattern in such a case may be prefer-

able to a sawtooth or triangular pattern that would be required for linear phase shifting.

The error analyses in this paper serve to illustrate the benefits of an algorithm design method for sinusoidal PSI based on the concept of balanced signal harmonics as described in Section 4 and an optimization tool based on the filter functions as described in Section 5. The results show that equivalent measurement performance is achievable with sinusoidal PSI in place of linear PSI for practical systems.

As a final note, an alternative approach described recently by Falaggis *et al.* relies on sampling the interference intensity during the approximately linear portions of the sinusoidal phase shift, enabling the use of more established linear phase shift algorithms [13]. This alternative also offers unique advantages for certain applications, depending on interferometer design and on the expected error sources.

References

1. D. Malacara, M. Servin, and Z. Malacara, *Interferogram Analysis for Optical Testing*, Vol. 61 of Optical Engineering Series (Marcel Dekker, 1998), pp. 169–245.
2. O. Sasaki, H. Okazaki, and M. Sakai, “Sinusoidal phase modulating interferometer using the integrating-bucket method,” *Appl. Opt.* **26**, 1089–1093 (1987).
3. O. Sasaki and H. Okazaki, “Analysis of measurement accuracy in sinusoidal phase modulating interferometry,” *Appl. Opt.* **25**, 3152–3158 (1986).
4. O. Sasaki, T. Okamura, and T. Nakamura, “Sinusoidal phase modulating Fizeau interferometer,” *Appl. Opt.* **29**, 512–515 (1990).
5. A. Dubois, “Phase-map measurements by interferometry with sinusoidal phase modulation and four integrating buckets,” *J. Opt. Soc. Am. A* **18**, 1972–1979 (2001).
6. X. Zhongbao and N. Zhang, “Sinusoidal phase modulation interferometer based on integration method,” *Proc. SPIE* **6357**, 635725 (2006).
7. P. J. de Groot and L. L. Deck, “New algorithms and error analysis for sinusoidal phase shifting interferometry,” *Proc. SPIE* **7063**, 706301 (2008).
8. P. de Groot, “Sinusoidal phase shifting interferometry,” U.S. patent application 2008/0180679 A1 (2008).
9. I. S. Gradshteyn and I. M. Ryzhik, *Table of Integrals, Series and Products* (Academic, 1980), p. 973.
10. P. Hariharan, B. F. Oreb, and T. Eiju, “Digital phase-shifting interferometry: a simple error-compensating phase calculation algorithm,” *Appl. Opt.* **26**, 2504–2506 (1987).
11. K. Freischlad and C. L. Koliopoulos, “Fourier description of digital phase-measuring interferometry,” *J. Opt. Soc. Am. A* **7**, 542–551 (1990).
12. P. de Groot, “Vibration in phase shifting interferometry,” *J. Opt. Soc. Am. A* **12**, 354–365 (1995).
13. K. Falaggis, D. P. Towers, and C. E. Towers, “Phase measurement through sinusoidal excitation with application to multi-wavelength interferometry,” *J. Opt. A Pure Appl. Opt.* **11**, 054008 (2009).